Nanoparticulate delivery systems for alkyl gallates: Influence of the elaboration process on particle characteristics, drug encapsulation and in-vitro release

Asma Chebil, Michèle Leonard, Jean-Luc Six, Cécile Nouvel, Alain Durand

Nanoparticulate delivery systems for alkyl gallates: influence of the elaboration process on particle characteristics, drug encapsulation and *in-vitro* release

Asma CHEBIL[1,2], Michèle LEONARD[1,2,*], Jean-Luc SIX[1,2], Cécile NOUVEL[1,2], Alain DURAND[1,2]

[1]CNRS, LCPM, UMR 7375, Nancy, F-54001, France

[2]Université de Lorraine, LCPM, UMR 7375, Nancy, F-54001, France

Statistical Summary: 8422 words, 3 figures, 5 tables.

[*] Corresponding author.

Email: mleonard@univ-lorraine.fr

Tel: 33 (0)3 83 17 52 76 / Fax: 33 (0)3 83 37 99 77

Graphical abstract

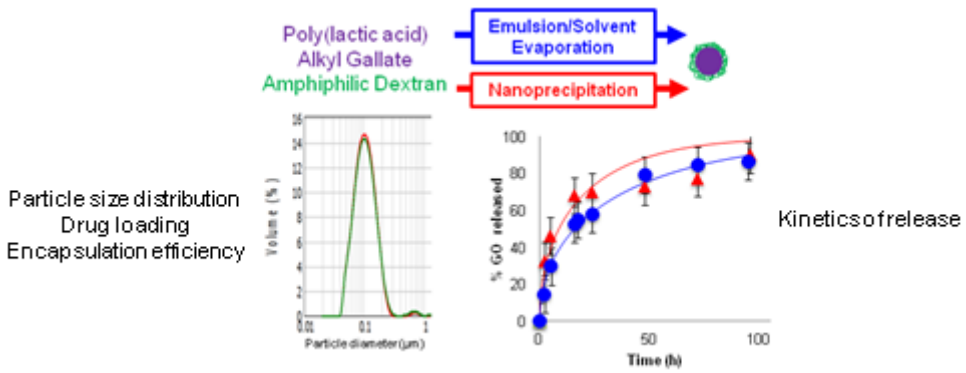

Highlights

- Dextran-covered poly(lactic acid) nanoparticles were loaded with n-alkyl gallates
- Emulsion/solvent evaporation (E/SE) and nanoprecipitation (NP) were compared
- The amount of encapsulated drug by E/SE was about twice that encapsulated by NP
- Drug release showed no burst effect and was controlled by diffusion in polymer core
- Diffusion of drug was slower within nanoparticles prepared by E/SE as compared to NP

ABSTRACT

PLA nanoparticles loaded with n-alkyl gallates (AGs) were prepared either by nanoprecipitation (NP) or by O/W emulsion/solvent evaporation (E/SE). A nonionic hydrophobically modified polysaccharide was used for surface coverage and for ensuring colloidal stability. Different parameters were systematically assessed to enhance the drug incorporation, with the aim of obtaining monomodal and narrow particle size distributions. The nanoparticles were characterized by ^{1}H NMR, transmission electron microscopy (TEM) and laser light scattering granulometry. The colloidal stability of suspensions was evaluated after incubation in NaCl solutions and was maintained up to 1 M NaCl. The mean particle diameter and the width of size distribution were found very similar for both processes (slightly lower diameters when using E/SE) with various drug loadings. The amount of encapsulated AG by E/SE was about twice that encapsulated by NP. The *in-vitro* release of AG was evaluated under sink conditions and no burst effect was observed. Release curves were successfully modeled using the Fick diffusion model with a constant diffusion coefficient and assuming non-swellable particles. Diffusion coefficients of AG loaded in

nanoparticles prepared by NP were higher than those found in nanoparticles elaborated by E/SE.

Keywords: Nanoparticles, Nanoprecipitation, Emulsion/Solvent Evaporation, Drug Release.

1. INTRODUCTION

There have been a lot of examples of formulations in which substances of interest among which hydrophobic molecules should be incorporated into mainly aqueous media [1,2]. A very common way to solve this difficulty has been encapsulating the hydrophobic active substance (AS) into polymeric nanoparticles [3-10]. Such nanoparticles could be dispersed into the aqueous phase and acted as reservoirs of hydrophobic ingredients increasing their available quantity per unit of volume by several orders of magnitude, much above their solubility limit in pure water. This formulation allowed continuous release of AS within the surrounding aqueous medium. Amongst physico-chemical properties, that should be considered for the encapsulation of AS into nanoparticles, several were deeply investigated: i) the size distribution and morphology of particles, ii) the drug loading, i.e. the amount of AS incorporated into nanoparticles (in weight fraction for instance), iii) the efficiency of encapsulation, i.e. the fraction of loaded drug that was included into the final particles, iv) the colloidal stability of the suspension of nanoparticles during the preparation of the formulation and under the conditions of application, v) the kinetics of release of AS out of the particles under the conditions of application, vi) the interactions between the surface of the particles and the surrounding medium (for instance for cell targeting strategies). Although a great deal of work has been reported about physico-chemical parameters controlling previous performances, less studies focused on the importance of the process of elaboration of suspensions [11-24]. This aspect appeared extremely important since the choice of the process

could have significant consequences both on the characteristics of nanoparticles and on the possibility of scaling up the production from lab scale to pilot scale [25,26]. The chemical characteristics of the surface of the particles may be controlled by covering the surface with defined sequences or functional groups via covalent attachment or physical interactions. In our laboratory, we particularly investigated the possibility of covering the surface of the particles by physically adsorbed or covalently linked layers of polysaccharides [27-32]. The polysaccharide layer, in addition to its biocompatibility and its contribution to colloidal stability, offered the possibility of further functionalization via covalent attachment of specific groups. In some instances polysaccharide layer was by itself selectively recognized by biological receptors [33].

Gallic acid and its esters, n-alkyl gallates (AGs), were well-known antioxidant molecules with various applications in many fields like medicine, cosmetics… [34,35] According to the nature of the alkyl group, AGs exhibited very different polarities and water solubilities [36-42]. Freeze dried microencapsulated sunflower oil and block copolymer micelles had been shown to allow encapsulation and release of gallic acid, and AGs covering a wide range of polarity [39,43]. Other strategies involved surface adsorption of gallic acid onto human serum albumin nanoparticles or polymer functionalization with gallic acid [44,45]. Nevertheless, to the best of our knowledge, encapsulation of AGs into polymeric nanoparticles had not been reported.

In that work, we investigated the encapsulation of two hydrophobic AGs, octyl gallate (OG) and nonyl gallate (NG), into nanoparticles of polylactic acid (PLA) covered by physical adsorption of hydrophobically modified dextran (**Figure 1a**). We particularly focused on the comparison of two physico-chemical processes of preparation: emulsion / solvent evaporation (E/SE) on the one hand and nanoprecipitation (NP) on the other hand. The effects of the

process on the particle size distribution, drug loading, efficiency of encapsulation and release kinetics have been studied experimentally following a systematic approach.

2. MATERIALS AND METHODS

2.1. *Materials*

D,L-poly(lactic acid) (PLA, $\overline{M_W}$ = 55,000 g/mol) and Dextran T40® (manufacturer data: weight average molar mass M_W 35-45,000 g/mol) were purchased from Sigma-Aldrich. The other chemicals were also purchased from Sigma-Aldrich. Dialysis membrane Spectra/Por (MWCO: 12-14 KD) was obtained from Spectrum laboratories Inc.

The hydrophobic derivatives of dextran ($DexC_6$-τ) were prepared as described previously [28]. The modified dextran was recovered by freeze drying and analyzed by ^{1}H NMR in DMSO-d_6 in which a few drops of D_2O were added. The substitution ratio τ (expressed in mol%) was defined by $\tau = 100 \times y/(x + y)$ where x was the number of moles of unmodified repeat units and y was the number of moles of covalently attached hydrocarbon tails contained in the polymer sample (**Figure 1a**). For substitution ratios up to 21 %, the solubility of dextran derivatives in water at 25 °C has been showed to exceed 100 g/L [46]. This was much higher than the concentration used in that work (10 g/L). The solubilities of AGs in water at 25 °C were determined experimentally (14 mg/L of OG and 8.6 mg/L for NG), by ^{1}H NMR in D_2O using phenol as reference. AGs were fully soluble in acetone and ethyl acetate within the range of concentrations explored in that work (up to 20 g/L).

2.2. *Processes for the preparation of nanoparticles* (**Figure 1b**)

2.2.1. O/W emulsion - solvent evaporation

An aqueous solution of $DexC_6$-τ (10 mL), was added into a solution of PLA + AG in ethyl acetate (EA, 2 or 5 mL). The concentration of $DexC_6$-τ in the aqueous phase was kept equal to

10 g/L for all experiments. The concentration of PLA + AG in EA was varied between 10 and 150 g/L. The mixture was pre-emulsified for 1 min using a vortex, then sonicated (pulsed mode, 50% active cycle) in an ice bath using a Bioblock Scientific vibracell 600W. The organic solvent was evaporated at 37°C in a ventilated oven for 1h30 min. Finally, the resulting suspension was centrifuged (25,000 g, 45 min), and the collected nanospheres were re-suspended in water then centrifuged again in order to remove the non-encapsulated AG and the non-adsorbed DexC_6-τ. The procedure was repeated 3 times. After freeze drying, the particles were analyzed by ^{1}H NMR in DMSO-d_6, in which a few drops of D_2O were added (in order to suppress signals from hydroxyl groups of sugar repeat units), to determine the amounts of adsorbed DexC_6-τ and encapsulated AG per g of PLA. In order to calculate the weight fraction of AG in nanoparticles the area of the peak of aromatic protons of AG (at 6.9 ppm) and the area of the proton from PLA repeat unit (at 5.2 ppm) were used (**Figure 1S Supplementary Material**). The relative uncertainty of this determination was ± 10 %.

2.2.2. Nanoprecipitation method

The solid mixture of PLA + AG was dissolved in 5 mL acetone. The concentration of PLA + AG in acetone was kept equal to 10 g/L for all experiments. Then the organic solution was added by mean of a syringe into 10 mL of an aqueous solution of DexC_6-τ (the needle was immersed into the aqueous solution). The concentration of DexC_6-τ in the aqueous phase was kept equal to 10 g/L for all experiments. The dispersing aqueous phase was magnetically stirred at 500 rpm. The particles were washed and characterized as described above for emulsion / solvent evaporation method (section 2.2.1).

2.3. *Miscibility of AGs and PLA*

Mixtures of PLA and AG were dissolved in 2 mL acetone. The solvent was evaporated in a ventilated oven at 37°C and the obtained solid samples were dried under vacuum for 24 h. The thermal transitions of PLA + AG solid mixtures were characterized by modulated differential scanning calorimetry (mDSC). The mDSC thermogramms (3 cycles) were recorded using a Q2000, TA Instruments apparatus. The heating rate was 5°C/min while the cooling rate was (10°C/min) under nitrogen, and the temperature was varied from -25°C up to 200°C. First MDSC cycle was used to remove all thermal history from the sample. Analysis of the data was performed using Universal® Analysis 2000 (version 4.5A) software.

2.4. *Particle characterization*

2.4.1. Size distribution and DexC$_6$-τ surface coverage

Particle size distribution was determined by laser light scattering (Mastersizer 2000© Malvern Instruments-Cellule: Hydro 2000µp) experiments. The laser granulometer used two laser sources with wavelengths equal to 633 nm and 466 nm. Light detectors were placed around the central point with a spatial arrangement following to a log-spaced array. Detectors covered an angular range between 0.015 and 144 degrees. Measurements were carried-out at 20 °C.
The broadness of the size distribution was qualified by the mean range of particle size (Span,

Equation (1))

$$Span = \frac{d(0.9) - d(0.1)}{d(0.5)} \quad \textbf{(1)}$$

where *d(0.9)*, *d(0.5)* and *d(0.1)* were the particle diameters at 90%, 50% and 10% cumulative volumes, respectively.

To the best of our knowledge, no universal interval has been adopted for *Span* values corresponding to a “monomodal” or a “multimodal” particle size distribution although it has been admitted that these two concepts (one quantitative and one qualitative) were related. Regarding the experimental results reported in that work, it appeared that monomodal distributions corresponded to *Span* values lower than 1.2. This limit was used for the discussion of the experimental results.

The average particle diameter was evaluated by the values of *d(0.5)* and by the surface mean diameter (D[3,2], **Equation (2)**).

$$D[3,2] = \frac{\sum_i n_i d_i^3}{\sum_i n_i d_i^2} \quad \textbf{(2)}$$

In **Equation (2)**, n_i was the number of particles with diameters equal to d_i (nm). The value of D[3,2] allowed calculation of the specific area of the particles (S_p, m^2/g) using the following formula: $S_p = 6/(\rho.D[3,2])$ in which ρ was the density of the particles (g/m^3).

The surface coverage of particles by $DexC_6$-τ (Γ, mg $DexC_6$-τ/m^2 particle) was calculated on the basis of ^1H NMR results and S_p values.

2.4.2. Dextran layer thickness

Electrophoretic mobility (μ_e) was determined in NaCl solutions as a function of ionic strength. The experiments were carried out on a Zetasizer 4 (Malvern Instruments, Malvern, UK). Zeta potential (ζ) was calculated from the electrophoretic mobility using the modified Booth equation [47]. This equation allowed the calculation of zeta potential for any k_H.R values, where k_H^{-1} was the Debye length and R the radius of particles, whereas the classical Smoluchowsky and Huckel's equations were only applicable under two limiting cases, i.e. k_H.R > 100 and k_H.R < 0.1 respectively. The electrokinetic layer thickness (Δ_{PZ}) were calculated from the zeta potential evolution vs k_H, using the Guy-Chapman equation (**Equation (3)**) [48].

$$Ln\left[\tanh\left(\frac{Ze\zeta}{4k_BT}\right)\right] = Ln\left[\tanh\left(\frac{Ze\psi_0}{4k_BT}\right)\right] - k_H \times \Delta_{PZ} \quad \textbf{(3)}$$

In **Equation (3)**, Z was the charge of Na^+Cl^- ions, e was the elementary charge of electron, k_B was the Boltzmann constant, Ψ_0 was the surface potential of particle and T was the absolute temperature.

2.4.3. Colloidal stability

The colloidal stability of latex suspensions in the presence of added electrolyte was assessed by turbidimetry. In a typical experiment, 0.5 mL of dispersions were added to 3.5 mL of NaCl solutions (from 10^{-4} to 4 M). The samples were allowed to stand for 1 h and their absorbance was measured over the range 450-700 nm, at 50-nm intervals. The slope *n* of the straight-line representing log (optical density) vs. log (wavelength) was taken as an indication of particle size [49]. The occurrence of flocculation upon increasing ionic strength was evidenced by a sharp decrease in *n* values.

2.4.4. In vitro AG release

Washed AG-loaded nanoparticle suspensions (about 35 mL) were separated in different aliquots of 4 mL and dialyzed against 2 L deionized water at ambient temperature. As the solubility of OG or NG in water was very low, the water phase was renewed three times per day to avoid a saturation of the solution and to ensure release in perfect sink conditions. At various intervals of time, aliquots were withdrawn and freeze dried. The amount of AG remaining in the particles was determined by ^{1}H NMR.

2.4.5. Morphological studies

Morphological examination of nanoparticles was performed by transmission electron microscopy (TEM) (Philips CM200, 200 KV, Institut Jean Lamour, UMR 7198, Nancy) following negative staining with uranyl acetate. The samples were prepared as follows: 100 µL of the final latex was diluted with 1 mL of deionized water. These diluted samples were then mounted on 400-mesh carbon-coated copper grids, a drop of uranyl acetate solution (2 wt% in ethanol) was added and the sample was then dried at room temperature.

Porosity of nanoparticles was estimated by comparing the specific surface area determined by laser granulometry and that obtained by BET measurements. Nitrogen sorption studies were performed using a Carlo Erba sorptomatic model 1900. Before measurements, the samples were degassed under vacuum at 80°C for 15 hours.

3. RESULTS AND DISCUSSION

3.1. *Selected processes for the preparation of AG-loaded nanoparticle suspensions*

The prepared nanoparticles consisted in a polymeric core made of poly(lactic acid) (PLA) covered by physically adsorbed polysaccharide chains (**Figure 1a**). The latter were prepared by chemical modification of dextran, a non ionic bacterial polysaccharide [28]. The corresponding polymers were named $DexC_6$-τ where τ was the molar ratio of attached hydrocarbon tails to the number of repeat units and was expressed in percents. Such polymers have been shown to ensure a dense surface coverage of PLA nanoparticles prepared by E/SE and NP [28,50]. Hydrophobic molecules, OG and NG, were encapsulated into the PLA core.

Two processes of preparation of nanoparticles were compared, nanoprecipitation (NP) and emulsion / solvent evaporation (E/SE), which were both divided into three unit operations (**Figure 1b**). During NP, PLA and AG were dissolved in acetone, a water-miscible solvent. The first unit operation of the NP process was the progressive addition of the previous organic solution into an aqueous solution of $DexC_6$-τ. Upon water-acetone interdiffusion, PLA and AG precipitated under the form of nanoparticles at the surface of which $DexC_6$-τ macromolecules adsorbed thus preventing the formation of aggregates. In the case of E/SE, PLA and AG were dissolved in ethyl acetate, a solvent with a limited miscibility with water (8.3 % v/v) [51]. The first unit operation of E/SE was emulsification of the previous organic solution into an aqueous phase containing $DexC_6$-τ by vortex mixing followed by sonication. The resulting submicronic oil droplets were stabilized by the adsorption of $DexC_6$-τ

macromolecules. For both processes (NP and E/SE), the second unit operation was organic solvent evaporation which led to solvent-free aqueous suspensions of solid nanoparticles. In the third process step nanoparticle suspensions were centrifuged and washed so as to eliminate non-encapsulated AG and non-adsorbed $DexC_6$-τ remaining in the aqueous phase. Final suspensions of AG-loaded dextran-covered PLA nanoparticles were further characterized regarding their size distribution, AG content, surface coverage, and colloidal stability.

3.2. *Influence of formulation variables on particle size distribution*

Nanoparticle size had been shown to influence both the biodistribution and the kinetics of drug release [52,53]. Therefore, this parameter had to be perfectly controlled and described. One aim of this work was the preparation of nanoparticle suspensions with narrow size distributions. The size distribution of particles was characterized using the *d(0.5)*, D[3,2] and span values (see Experimental for details). In the case of monomodal and narrow size distributions, we found that the Span values lied within the range 0.8-1.4. Span values higher than 1.5 were considered as characteristic of broad size distributions, with mixtures of submicrometric and micrometric particles.

We first investigated the effect of process and formulation parameters on the size distribution of PLA nanoparticles.

3.2.1. Effect of $DexC_6$-τ substitution ratio on the colloidal stability of nanoparticle suspensions

PLA nanospheres in the size range 80-140 nm could be prepared either by NP or E/SE methods using hydrophobically modified dextrans $DexC_6$-τ as stabilizers, with substitution ratios between 14 and 22 % (**Table 1**). Except for τ = 22 %, the obtained Span values were

characteristic of monomodal and narrow particle size distributions. PLA nanoparticle suspensions elaborated using a $DexC_6$-τ with substitution ratio higher than 20 % were not stable in NaCl solutions, despite similar amounts of adsorbed $DexC_6$-τ (**Table 1**). This has been explained by an excess of hydrophobic tails that were not in contact with the PLA surface but accumulated within the polymeric loops extending in the external aqueous solution [54]. These hydrocarbon groups either gave rise to attractive hydrophobic interactions between nanoparticles, as soon as the suspension was concentrated by centrifugation, or induced a compaction of the superficial layer when the ionic strength of the aqueous medium was increased. Thus only the $DexC_6$-τ with substitution ratios between 14 % and 20 % were used as stabilizers for the following experiments.

3.2.2. Optimization of conditions for the elaboration of PLA nanoparticles.

When the NP process was used, it was not possible to prepare suspensions having monomodal particle size distributions (with *Span* values lower than 1.2) with PLA concentrations higher than 15 mg/ mL in acetone (**Table 1S Supplementary Material**). Despite an extensive study of NP process parameters (organic to water phase ratio, $DexC_6$-τ concentration, position of the syringe, agitation speed…), PLA concentrations above this value led to the formation of aggregates or films in the aqueous solution. Similar results were obtained by Legrand et al. who systematically investigated the influence of PLA molar mass and concentration in acetone on the average diameter of particles produced by nanoprecipitation [55]. In addition, this concentration range was similar to that used with other polymer-solvent systems for nanoprecipitation [12]. In the case of polymer solutions, it has been usual to distinguish dilute domain and semi-dilute domain according to polymer concentration. For polymer concentrations lower than the critical overlap concentration (C*), macromolecular coils remained isolated and independent from each other. For polymer concentrations higher than

C*, polymer coils overlapped and entangled. It has been shown that C* was roughly inversely proportional to the intrinsic viscosity of the polymer in the solvent. From the viscometric measurements of Legrand et al. we could estimate that the overlap concentration of the PLA sample in acetone was roughly 19 mg/mL. This showed that for the NP process, dilute solutions of PLA in acetone have to be used to obtain monomodal particle size distributions.

Conversely, for E/SE process, PLA solutions with much higher concentrations (up to 150 mg/mL in ethyl acetate) could be used while keeping monomodal particle size distributions. The upper limitation of 150 mg/mL was attributed to the viscosity of the PLA solution, on the basis of visual observations. On the basis of literature data, the overlap concentration of our PLA sample in EA was roughly identical to that estimated in acetone [56]. Thus, the upper limitation of PLA concentration was about 10 times the overlap concentration, which corresponded to the semi-dilute entangled domain [57]. As a conclusion, for E/SE process, PLA concentration in the organic phase was limited by the viscosity range compatible with formation of submicrometric droplets.

Consequently, the concentration of PLA in the organic phase should be much lower in case of NP process as compared to E/SE. These results were consistent with the conclusions of Mora-Huertas et al. who reviewed literature data about nanoparticle preparation by both processes [12].

Finally, for all encapsulation experiments using NP, the amount of PLA and AG in acetone was kept equal to 10 mg/mL. In the case of E/SE process, the amount of PLA and AG in ethyl acetate was varied between 50 and 150 mg/mL.

3.3. *Optimization of conditions for the elaboration of AG-loaded nanoparticles.*

We first studied the miscibility of octyl gallate (OG) and nonyl gallate (NG) with PLA by examining the thermal transitions of PLA + AG solid mixtures by m-DSC (see Experimental).

Both AGs were miscible with PLA up to OG weight fractions (W_{OG}) ~ 30 % (w/w) and NG weight fractions (W_{NG}) ~ 25 % (w/w). Within that range of AG weight fractions, solid mixtures exhibited a single thermal transition characterized by one glass transition temperature (T_g). In addition, the T_g of the PLA + AG mixtures decreased upon increasing W_{AG} which was attributed to the plasticizing effect of AGs (**Figure 2S Supplementary Material**). Experimental T_g were compared to estimations based on Fox equation (**Equation (4)**) [58].

$$\frac{1}{T_{g\,mixture}} = \frac{W_{PLA}}{T_{g\,PLA}} + \frac{W_{AG}}{T_{g\,AG}} \qquad \textbf{(4)}$$

In **Equation (4)**, $T_{gmixture}$, T_{gPLA}, and T_{gAG} were the glass transition temperatures (K) of PLA-AG mixture, bulk PLA and AG, respectively, W_{PLA} and W_{AG} were the weight fractions of PLA and AG in PLA + AG mixture, respectively. Experimental values of T_{gAG} were not available and were estimated from the melting temperatures of AGs (**Equation (5)**). This equation had been shown to provide reasonable estimations for molecular liquids as well as for polymers [59,60].

$$T_{g\,AG} \cong \frac{2}{3} T_{m\,AG} \qquad \textbf{(5)}$$

In **Equation (5)**, T_{mAG} was the melting temperature of AG (K).

For mixtures with $W_{OG} \leq 30$ % or $W_{NG} \leq 25$ %, the estimated T_g values were in good agreement with experimental values (**Figure 2S Supplementary Material**), which supported the idea of molecular dispersion of AGs within PLA chains giving rise to plasticizing effect. To the best of our knowledge, this is the first report about plasticizing effect of AGs.

For PLA + AG mixtures containing $W_{OG} > 30$ % or $W_{NG} > 25$ % fusion endotherms of AGs were observed, and a significant deviation of experimental T_g values from estimations with **Equation (4)** was observed (**Figure 2S Supplementary Material**). These results were interpreted as a consequence of phase separation between an amorphous PLA-rich phase and

a crystalline AG phase. Similar results have been reported about mixtures of poly(DL-lactide) and citrate esters [61].

The effect of formulation parameters on the size distribution of OG- and NG-loaded PLA nanoparticles obtained by NP or E/SE was systematically investigated (**Table 2a**, **2b** and **2c**). When W_{AG} in the load was higher than 20 % (resp. 30 %) w/w in case of E/SE (resp. NP) process, the particle size distributions became significantly broader (the Span increased dramatically) after the centrifugation and washing steps. The same phenomenon was observed when the amount of PLA + AG in the organic phase was increased at a given weight ratio (as illustrated for E/SE process in **Table 2b**). In addition, the surface coverage by $DexC_6$-τ did not significantly vary for all the explored conditions and for both processes. These results showed that limited aggregate formation occurred during the centrifugation and washing steps despite the superficial layer of $DexC_6$-τ when the solid content of the suspension was higher than 1 wt% (NP) or 10 wt% (E/SE) and when the loaded amount of AG exceeded 20 wt% (E/SE) or 30 wt% (NP) compared to the total PLA + AG amounts. The latter effect was attributed to the plasticizing effect of AG which led to particles with soft cores and favored the formation of aggregates during centrifugation steps. As a conclusion, for both processes, regarding the loaded amount and the composition of the PLA + AG mixture in the organic phase, the main limitation concerned aggregation phenomena during centrifugation and washing steps and not the two preceding unit operations (particle elaboration and solvent evaporation).

The performances of encapsulation of OG and NG in nanoparticles by both processes were characterized by determining the drug loading (in mg of AG/g PLA in final particles), and the encapsulation efficiency (EE, fraction of loaded AG present in final particles) for all explored conditions (**Figure 2**). The EE was lower than 25 % in case of NP and between 18 and 70 % in case of E/SE. These rather low values of encapsulated AG were attributed to the increased

solubilities of OG and NG in the aqueous phase, due to the presence of $DexC_6$-τ in the aqueous phase. For both processes, when increasing W_{AG} in the organic phase, the EE decreased while the drug loading increased as well as the Span of size distribution of final particles. In the case of E/SE process, increasing the loaded amount of PLA + AG in ethyl acetate led to an increase of EE as well as drug loading into final particles. Nevertheless, the Span of particle size distribution also increased (**Table 2b**).

In order to evaluate the effects of the process and of the AG structure on the performances of encapsulation, we plotted the amount of encapsulated AG (in mg / g PLA) as a function of the non-encapsulated AG remaining in the aqueous phase before washing (in mg / g of aqueous phase) which was calculated on the basis of a simple mass balance (**Figure 3S Supplementary Material**). We observed reasonably linear variations for both AGs and both processes. The slopes of the curves were used for quantitative comparison of encapsulation performances and were assimilated to "overall partition coefficients" (noted K_p, **Table 3**). Indeed, we assumed that during nanoparticle elaboration, AG exchanges between organic phase and aqueous medium were stopped when solid nanoparticles formed. In the case of NP, the formation of solid nanoparticles corresponded to the co-precipitation of AG and PLA upon acetone-water interdiffusion and in the case of E/SE this took place during ethyl acetate evaporation. Thus the value of K_p was indicative of the partition of AGs between inner particle core and outer aqueous medium. All values were found between 31 and 46 except for NG during E/SE process for which the value was 69, showing a significantly more efficient encapsulation. In the case of NP process, OG and NG exhibited similar values of K_p which indicated similar affinities for PLA. For the encapsulation of OG, NP and E/SE exhibited similar efficiencies regarding the loss of non-encapsulated active substance into the external aqueous phase. Nevertheless, for NG, the use of E/SE was more efficient than NP. The use of

ethyl acetate favored the partition of NG into the PLA-rich core as compared to the co-precipitation which occurred during NP process.

The amount of OG and NG that could be encapsulated in particles prepared by E/SE was approximately two times higher than the amount of OG and NG which could be encapsulated in particles prepared by NP. The higher drug loading, as determined by ^{1}H NMR for monomodal particles, were 55 mg/g PLA, ±10% for OG3-NP, 38.8 mg/g PLA, ±10% for NG3-NP, 101 mg/g PLA, ±10% for OG4-E/SE and 84 mg/g PLA, ±10% for NG3-E/SE. This was explained on the basis of the previously discussed partition phenomenon and by the fact that more concentrated PLA + AG organic solutions could be used for preparing well-defined nanoparticles by E/SE than those used in the NP process.

Finally, we carried out a direct comparison of NG encapsulation using either NP or E/SE process with exactly the same formulation parameters except the nature of the organic solvent (**Table 2c**). Particles produced by NP process exhibited slightly higher diameters and lower EE, as compared to those obtained by E/SE process. The result about EE was consistent with previous discussion about K_p values. Other properties were characterized, surface coverage by $DexC_6$-18, thickness of $DexC_6$-18 layer as well as colloidal stability, and were found very similar for nanoparticles produced by both processes. TEM images of both types of nanoparticles confirmed that the obtained particles had uniform and spherical shape. Average diameters estimated from TEM images were in agreement with data obtained by laser granulometry (**Figure 4S Supplementary Material**). Laser granulometry, provided d(0.5) value of 96 nm which corresponded to the PLA hard core surrounded by the soft dextran layer whose thickness was of the order of 10 nm. The TEM images showed particles with diameters between 60 and 90 nm, which were fully consistent with the results of laser granulometry.

3.4. *In vitro release*

The release profiles of OG and NG from nanoparticles elaborated by E/SE and NP under similar conditions were compared (**Figure 3a** and **3b**). The profiles did not show any burst release effect. A power-law equation (**Equation (6)**) was applied to the first 60 % fractional release [62].

$$\frac{M_t}{M_\infty} = k\,t^{\alpha} \qquad \textbf{(6)}$$

In **Equation (6)**, M_t and M_∞ were the masses (g) of drug released at instant t and after infinite time, respectively. k was a constant and α was the diffusional exponent which was characteristic of the release mechanism. We found a rather satisfactory agreement between experimental and calculated curves with $\alpha = 0.43$ (**Figure 3a and 3b, inset**), which had been shown to characterize release out of isometric spheres through Fickian diffusion [62].

Consequently, the release profiles were modeled using the Fick diffusion model under the assumptions of perfect sink initial and boundary conditions and constant diffusion coefficient (D) (**Equation (7)**) [63].

$$\frac{M_t}{M_\infty} = 1 - \frac{6}{\pi^2}\sum_{n=1}^{\infty}\frac{1}{n^2}\exp\left[-\frac{Dn^2\pi^2 t}{R^2}\right] \qquad \textbf{(7)}$$

In **Equation (7)**, D was the diffusion coefficient of AG (m^2/s), t was the time (s), R was the radius of the nanoparticles (m) and n was an integer.

We preferred to use a single model for all experiments so that one physical parameter like diffusion coefficient could be extracted and compared according to particle preparation rather than using several fitting equations so as to improve curve fitting for each data series separately.

Diffusion coefficients of both AGs from nanoparticles at different drug loading and prepared by NP or E/SE were calculated (**Table 4a**). The found values of diffusion coefficients were between 0.1 10^{-21} and 6.5 10^{-21} m^2/s, which was consistent with previously reported values for the release of hydrophobic substances out of PLA particles prepared either by NP or by E/SE

(**Table 4b**). Three main tendencies could be evidenced from calculated values of diffusion coefficients. First, for similar drug loadings, diffusion coefficient of OG was higher than that of NG. This could be attributed to less favorable interactions between NG and PLA matrix as compared to OG. Other data would be necessary for a more detailed discussion of that point. Secondly, for particles prepared by the same process (NP or E/SE), the diffusion coefficient did not vary significantly with the drug loading. This was an indication that OG and NG were uniformly distributed within the PLA matrix, with no accumulation near the particle surface. Finally, for similar drug loadings, the kinetics of release of OG and NG out of nanoparticles prepared by NP led to higher values of diffusion coefficients than those found for the release out of nanoparticles prepared by E/SE. These results about faster release from nanoparticles produced by nanoprecipitation as compared to E/SE were consistent with other observations about release of hydrophobic drugs as well as hydrophilic drugs (for which double emulsion evaporation process was used) [16,18,19]. BET isotherms were established with freeze-dried samples of suspensions of nanoparticles prepared either by NP or by E/SE process. These experiments showed that all samples were macroporous materials and thus, whatever the process of preparation, no porosity within the nanoparticles could be evidenced. Thus the effect of the process of preparation on the diffusion coefficient was not a consequence of the formation of pores and might result from differences at the scale of macromolecules (like free volume for instance).

4. CONCLUSION

Alkyl gallate-loaded nanoparticles of poly(lactic acid) have been prepared by two processes, nanoprecipitation and emulsion/solvent evaporation. For both processes, the surface of nanoparticles was covered by dextran loops via the use of hydrophobically modified dextran derivatives as stabilizers during the formation of nanoparticles. Processes were compared

regarding particle size distribution and performances of encapsulation and release of octyl gallate and nonyl gallate. In both cases very similar nanoparticles were produced in terms of size distribution, surface coverage, and colloidal stability as a function of ionic strength. In addition, both processes were limited regarding the maximum drug content in the load, which was attributed to aggregation during washing operations. Nanoparticles with higher drug loadings could be obtained using the emulsion/solvent evaporation process. Release kinetics was satisfactorily described by Fickian diffusion mechanism for both drugs and for particles prepared by both processes. Nevertheless, drug release was faster for nanoparticles prepared by the nanoprecipitation process.

Current work explores the surface functionalization of nanoparticles for targeting active substances.

Acknowledgements

The authors gratefully acknowledge the financial support of Région Lorraine and European Union (FEDER) to the BioCapTech project (PhD of AC). Loïc Chomel de Varagnes and Jean-Claude Pihan (BioCapTech Company) are acknowledged for many fruitful discussions.

References

[1] B. Liebmann, D. Huemmerich, T. Scheibel, M. Fehr, Formulation of poorly water-soluble substances using self-assembling spider silk protein, Colloids and Surfaces A 331 (2008) 126-132.

[2] F. Zhang, J.C. DiNunzio. in *Formulating poorly water soluble drugs*; R. O. Williams, A. B. Wattsand D. A. Miller, Eds., 2012, p 171-208.

[3] I. Katouzian, S.M. Jafari, Nano-encapsulation as a promising approach for targeted delivery and controlled release of vitamins, Trends Food Sci. Technol. 53 (2016) 34-48.

[4] C. Wischke, S.P. Schwendeman, Principles of encapsulating hydrophobic drugs in PLA/PLGA microparticles, Int. J. Pharm. 364 (2008) 298-327.

[5] J.A. Tapia-Hernandez, P.I. Torres-Chavez, B. Ramirez-Wong, A. Rascon-Chu, M. Plascencia-Jatomea, C.G. Barreras-Urbina, N.A. Rangel-Vazquez, F. Rodriguez-Felix, Micro- and Nanoparticles by Electrospray: Advances and Applications in Foods, J. Agric. Food Chem. 63 (2015) 4699-4707.

[6] V. Lassalle, M.L. Ferreira, PLA Nano- and Microparticles for Drug Delivery: An Overview of the Methods of Preparation, Macromol. Biosci. 7 (2007) 767-783.

[7] F. Masood, Polymeric nanoparticles for targeted drug delivery system for cancer therapy, Mat. Sci. Eng. C 60 (2016) 569-578.

[8] Y. Wang, P. Li, T.T.-D. Tran, J. Zhang, L. Kong, Manufacturing Techniques and Surface Engineering of Polymer Based Nanoparticles for Targeted Drug Delivery to Cancer, Nanomaterials 6 (2016) 26.

[9] M. Izadifar, M.E. Kelly, A. Haddadi, X. Chen, Optimization of nanoparticles for cardiovascular tissue engineering, Nanotechnology 26 (2015) 235301.

[10] C.E. Mora-Huertas, H. Fessi, A. Elaissari, Polymer-based nanocapsules for drug delivery, Int. J. Pharm. 385 (2010) 113-142.

[11] S.A. Guhagarkar, V.C. Malshe, P.V. Devarajan, Nanoparticles of Polyethylene Sebacate: A New Biodegradable Polymer, AAPS PharmSciTech 10 (2009) 935-942.

[12] C.E. Mora-Huertas, H. Fessi, A. Elaissari, Influence of process and formulation parameters on the formation of submicron particles by solvent displacement and emulsification–diffusion methods Critical comparison, Adv. Colloid Interface Sci. 163 (2011) 90-122.

[13] C. Prashant, M. Dipak, C.-T. Yang, K.-H. Chuang, D. Jun, S.-S. Feng, Superparamagnetic iron oxide - Loaded poly (lactic acid)–D-α-tocopherol polyethylene glycol 1000 succinate copolymer nanoparticles as MRI contrast agent, Biomaterials 31 (2010) 5588-5597.

[14] A. Sano, T. Kuriki, Y. Kawashima, H. Takeuchi, T. Hino, T. Niwa, Particle design of Tolbutamide by the spherical crystallization technique. III. Micromeritic properties and dissolution rate of Tolbutamide spherical agglomerates prepared by the quasi-emulsion solvent diffusion method and the solvent change method, Chem. Pharm. Bull. 38 (1990) 733-739.

[15] K.P. Seremeta, D.A. Chiappetta, A. Sosnik, Poly(-caprolactone), Eudragit® RS 100 and poly(-caprolactone)/Eudragit® RS 100 blend submicron particles for the sustained release of the antiretroviral efavirenz, Colloids Surf. B: Biointerfaces 102 (2013) 441-449.

[16] S. Han, M. Li, X. Liu, H. Gao, Y. Wu, Construction of amphiphilic copolymer nanoparticles based on gelatin as drug carriers for doxorubicin delivery, Colloids Surf. B: Biointerfaces 102 (2013) 833-841.

[17] C.E. Mora-Huertas, O. Garrigues, H. Fessi, A. Elaissari, Nanocapsules prepared via nanoprecipitation and emulsification–diffusion methods: Comparative study, Eur. J. Pharm. Biopharm. 80 (2012) 235-239.

[18] K. Miladi, S. Sfar, H. Fessi, A. Elaissari, Encapsulation of alendronate sodium by nanoprecipitation and double emulsion: From preparation to in vitro studies, Ind. Crops Products 72 (2015) 24-33.

[19] R. Saadati, S. Dadashzadeh, Marked effects of combined TPGS and PVA emulsifiers in the fabrication of etoposide-loaded PLGA-PEG nanoparticles: In vitro and in vivo evaluation, Int. J. Pharm. 464 (2014) 135-144.

[20] M. Kanani, K. Vadalia, Formulation, Evaluation and Comparison of Exemestane Nanoparticles Prepared by Nanoprecipitation Method and Spontaneous Emulsification Solvent Diffusion Method, Int. J. Pharm Tech Res. 8 (2015) 236-249.
[21] S. Galindo-Rodriguez, E. Allémann, E. Doelker, H. Fessi, Versatility of three techniques for preparing ibuprofen-loaded methacrylic acid copolymer nanoparticles of controlled sizes, J. Drug Del. Sci. Tech. 15 (2005) 347-354.
[22] S.A. Abdel Halim, S. Salah, Development of nanoparticulate formulations for ocular delivery of prednisolone acetate: preparation and characterization, J. Drug Del. Sci. Tech. 24 (2014) 159-165.
[23] C.E. Mora-Huertas, F. Couenne, H. Fessi, Electrokinetic properties of poly-e-caprolactone-based nanoparticles prepared by nanoprecipitation and emulsification-diffusion methods: a comparative study, J. Nanopart. Res. 14 (2012) 876-890.
[24] S. Galindo-Rodriguez, E. Allémann, H. Fessi, E. Doelker, Physicochemical Parameters Associated with Nanoparticle Formation in the Salting-out, Emulsification-Diffusion, and Nanoprecipitation Methods, Pharm. Res. 21 (2004) 1428-1439.
[25] S.A. Galindo-Rodriguez, F. Puel, S. Briançon, E. Allémann, E. Doelker, H. Fessi, Comparative scale-up of three methods for producing ibuprofen-loaded nanoparticles, Eur. J. Pharm. Sci. 25 (2005) 357-367.
[26] C. Vauthier, K. Bouchemal. in *Intracellular Delivery: Fundamentals and Applications, Fundamental Biomedical Technologies*; A. Prokop, Ed.; Springer Science+Business Media B. V., 2011, p 433-456.
[27] M. Laville, J. Babin, I. Londono, M. Legros, C. Nouvel, A. Durand, R. Vanderesse, M. Léonard, J.-L. Six, Polysaccharide-covered nanoparticles with improved shell stability using click-chemistry strategies, Carbohydr. Polym. 93 (2013) 537-546.
[28] C. Rouzes, M. Léonard, A. Durand, E. Dellacherie, Influence of polymeric surfactants on the properties of drug-loaded PLA nanospheres, Colloids and Surfaces B 32 (2003) 125-135.
[29] H. Laroui, L. Grossin, M. Leonard, J.-F. Stoltz, P. Gillet, P. Netter, E. Dellacherie, Hyaluronate-Covered Nanoparticles for the Therapeutic Targeting of Cartilage, Biomacromolecules 8 (2007) 3879-3885.
[30] K. Poltorak, A. Durand, M. Léonard, J.-L. Six, C. Nouvel, Interfacial click chemistry for improving both dextran shell density and stability of biocompatible nanocapsules, Colloids Surf. A: Physicochem. Eng. Aspects 483 (2015) 8-17.
[31] C. Nouvel, J. Raynaud, E. Marie, E. Dellacherie, J.-L. Six, A. Durand, Biodegradable nanoparticles made from polylactide-grafted dextran copolymers, J. Colloid Interface Sci. 330 (2009) 337-343.
[32] L.M. Forero, J. Babin, A. Durand, J.-L. Six, C. Nouvel, Biocompatible dextran-covered nanoparticles produced by activator generated by electron transfer atom transfer radical polymerization in miniemulsion, Colloids Surf. A: Physicochem. Eng. Aspects 486 (2015) 60-68.
[33] H. Zille, J. Paquet, C. Henrionnet, J. Scala-Bertola, M. Leonard, J.-L. Six, F. Deschamps, P. Netter, J. Verges, P. Gillet, L. Grossin, Evaluation of intra-articular delivery of hyaluronic acid functionalized biopolymeric nanoparticles in healthy rats knees, Biomed. Mater. Eng. 20 (2010) 235-242.
[34] V.G. Wolf, C. Bonacorsi, M.S.G. Raddi, L.M. da Fonseca, V.F. Ximenes, Octyl gallate, a food additive with potential beneficial properties to treat Helicobacter pylori infection, Food & Function 8 (2017) 2500-2511.
[35] J.M. Kratz, C.R. Andrighetti-Frohner, P.C. Leal, R.J. Nunes, R.A. Yunes, E. Trybala, T. Bergstrom, C.R.M. Baradi, C.M.O. Simoes, Evaluation of anti-HSV-2 activity of gallic acid and pentyl gallate, Biol. Pharm. Bull. 31 (2008) 903-907.
[36] R. Rosso, T.O. Vieira, P.C. Leal, R.J. Nunes, R.A. Yunes, T.B. Creczynski-Pasa, Relationship between the lipophilicity of gallic acid n-alquil esters'derivatives and both myeloperoxidase activity and HOCl scavenging, Bioorg. Med. Chem. 14 (2006) 6406-6413.
[37] E. Sergediene, K. Jönsson, H. Szymusiak, B. Tyrakowska, I.M.C.M. Rietjens, N. Cenas, Prooxidant toxicity of polyphenolic antioxidants to HL-60 cells: description of quantitative structure-activity relationships, FEBS Lett. 462 (1999) 392-396.

[38] S.L. Barreiro, C. Bravo-Diaz, F. Paiva-Martins, L.S. Romsted, Maxima in Antioxidant Distributions and Efficiencies with Increasing Hydrophobicity of Gallic Acid and Its Alkyl Esters. The Pseudophase Model Interpretation of the "Cutoff Effect", J. Agric. Food Chem. 61 (2013) 6533-6543.
[39] J. Velasco, F. Holgado, C. Dobarganes, G. Marquez-Ruiz, Antioxidant Activity of Added Phenolic Compounds in Freeze-Dried Microencapsulated Sunflower Oil, J. Am. Oil Chem. Soc. 86 (2009) 445-452.
[40] L.S.C. Wan, C.L. Hwang, Antioxidant Solubility and Efficiency, J. Pharm. Sci. 58 (1969) 889-891.
[41] M. Shalini, T. Kalaivani, C. Rajasekaran. in *Recent Advances in Gallate Research*; A. L. Kinsey, Ed.; Nova Science Publishers, Inc., 2014.
[42] O.S. Maldonado, R. Lucas, F. Comelles, M.J. Gonzalez, J.L. Parra, I. Medina, J.C. Morales, Synthesis and characterization of phenolic antioxidants with surfactant properties: glucosyl- and glucuronosyl alkyl gallates, Tetrahedron 67 (2011) 7268-7279.
[43] I. Fuentes, B. Blanco-Fernandez, N. Alvarado, A. Leiva, D. Radic, C. Alvarez-Lorenzo, A. Concheiro, Encapsulation of Antioxidant Gallate Derivatives in Biocompatible Poly(ε-caprolactone)‑ b‑ Pluronic‑ b‑ Poly(ε-caprolactone) Micelles, Langmuir 32 (2016) 3331-3339.
[44] H. Mohammad-Beigi, S.A. Shojaosadati, D. Morshedi, A. Arpanaei, A.T. Marvian, Preparation and in vitro characterization of gallic acid-loaded human serum albumin nanoparticles, J. Nanopart. Res. 17 (2015) 167-182.
[45] J.-Y. Lai, L.-J. Luo, Antioxidant Gallic Acid-Functionalized Biodegradable in Situ Gelling Copolymers for Cytoprotective Antiglaucoma Drug Delivery Systems, Biomacromolecules 16 (2015) 2950-2963.
[46] E. Rotureau, C. Chassenieux, E. Dellacherie, A. Durand, Neutral polymeric surfactants derived from dextran: a study of their aqueous solution behavior, Macromol. Chem. Phys. 206 (2005) 2038-2046.
[47] S.R. Deshiikan, K.D. Papadopoulos, Modified Booth equation for the calculation of zeta potential Colloid Polym. Sci. 276 (1998) 117-124.
[48] W.G. Eversole, W.W. Boardman, The effect of electrostatic forces on electrokinetic potentials, J. Chem. Phys. 9 (1941) 798-801.
[49] J.A. Long, D.W.J. Osmond, B. Vincent, The equilibrium aspects of weak flocculation, J. Colloid Interface Sci. 42 (1973) 545-553.
[50] C. Gavory, A. Durand, J.-L. Six, C. Nouvel, E. Marie, M. Léonard, Polysaccharide-covered nanoparticles prepared by nanoprecipitation, Carbohydr. Polym. 84 (2011) 133-140.
[51] M.d.C. Grande, C.M. Marschoff, Liquid-Liquid Equilibria for Water + Benzonitrile + Ethyl Acetate or + Butyl Acetate, J. Chem. Eng. Data 50 (2005) 1324-1327.
[52] P. Stloukal, P. Kucharczyl, V. Sedlarik, P. Bazant, M. Koutny, Low molecular weight poly(lactic acid) microparticles for controlled release of the herbicide Metazachlor: Preparation, Morphology, and Release Kinetics, J. Agric. Food Chem. 60 (2012) 4111-4119.
[53] V.P. Venkatpurwar, S. Rhodes, K.A. Oien, M.A. Elliott, C.D. Tekwe, H.G. Jorgensen, M.N.V.R. Kumar, Drug-not-carrier-dependent haematological and biochemical changes in a repeated dose study of cyclosporine encapsulated polyester nano- and microparticles, Toxicology 330 (2015) 9-18.
[54] C. Fournier, M. Leonard, E. Dellacherie, M. Chikhi, H. Hommel, A.P. Legrand, EPR spectroscopy analysis of hydrophobically modified dextran-coated polystyrene, J. Colloid Interface Sci. 198 (1998) 27-33.
[55] P. Legrand, S. Lesieur, A. Bochot, R. Gref, W. Raatjes, G. Barratt, C. Vauthier, Influence of polymer behaviour in organic solution on the production of polylactide nanoparticles by nanoprecipitation, Int. J. Pharm. 344 (2007) 33-43.
[56] D. Garlotta, A Literature Review of Poly(Lactic Acid), J. Polym. Environment 9 (2001) 63-84.
[57] W.W. Graessley, Polymer chain dimensions and the dependence of viscoelastic properties on concentration, molecular weight and solvent power, Polymer 21 (1980) 258-262.
[58] T.G. Fox, Influence of diluent and of copolymer composition on the glass temperature of a polymer system, Bull. Am. Phys. Soc. 1 (1956) 123.

[59] C.A. Angell, J.M. Sare, E.J. Sare, Glass Transition Temperatures for Simple Molecular Liquids and Their Binary Solutions, J. Phys. Chem. 82 (1978) 2622-2629.
[60] W.A. Lee, G.J. Knight, Ratio of the glass transition temperature to the melting point in polymers, Br. Polym. J. 2 (1970) 73-80.
[61] I. Harte, C. Birkinshaw, E. Jones, J. Kennedy, E. DeBarra, The Effect of Citrate Ester Plasticizers on the Thermal and Mechanical Properties of Poly(DL-lactide), J. Appl. Polym. Sci. 127 (2013) 1997-2003.
[62] P.L. Ritger, N.A. Peppas, Simple equation for description of solute release I. Fickian and non-Fickian release from non-swellable devices in the form of slabs, spheres, cylinders or discs, J. Controlled Release 5 (1987) 23-36.
[63] R.H. Guy, J. Hadgraft, I.W. Kellaway, M.J. Taylor, Calculations of drug release rates from spherical particles, Int. J. Pharm. 11 (1982) 199-207.
[64] A. Budhian, S.J. Siegel, K.I. Winey, Controlling the in vitro release profiles for a system of haloperidol-loaded PLGA nanoparticles, Int. J. Pharm. 346 (2008) 151-159.
[65] M. Polakovic, T. Görner, R. Gref, E. Dellacherie, Lidocaine loaded biodegradable nanospheres II. Modelling of drug release, J. Control. Release 60 (1999) 169-177.
[66] M.S. Romero-Cano, B. Vincent, Controlled release of 4-nitroanisole from poly(lactic acid) nanoparticles, J. Control. Release 82 (2002) 127-135.
[67] M. Chorny, I. Fishbein, H.D. Danenberg, G. Golomb, Study of the drug release mechanism from tyrphostin AG-1295-loaded nanospheres by in situ and external sink methods, J. Control. Release 83 (2002) 401-414.

Figure captions

Figure 1a: Chemical structure of DexC_6-τ, alkyl gallates, PLA, and targeted structure of nanoparticles.

Figure 1b: Nanoprecipitation and emulsion/solvent evaporation processes used for preparing nanoparticles.

Figure 2: Encapsulation data of OG and NG in nanoparticles prepared by NP (a, b) and E/SE (c, d). Black bars: Drug loading (mg/g PLA). White bars: Encapsulation efficiency (%). See **Table 3** and **4** for the conditions of preparation. Each experiment was repeated between 2 and 3 times (n = 2 to 3, ± SD with SD between 8 and 10 %).

Figure 3a: Release profiles of OG and NG from OG2-E/SE (●) and NG2-E/SE (▲) particles. Curve fit: see text. Each experiment was repeated between 2 and 3 times (n = 2 to 3, ± SD with SD between 6 and 9 %).

Figure 3b: Release profiles of OG and NG from OG2-NP (●) and NG2-NP (▲) particles. Curve fit: see text. Each experiment was repeated between 2 and 3 times (n = 2 to 3, ± SD with SD between 8 and 10 %).

Figure 1a

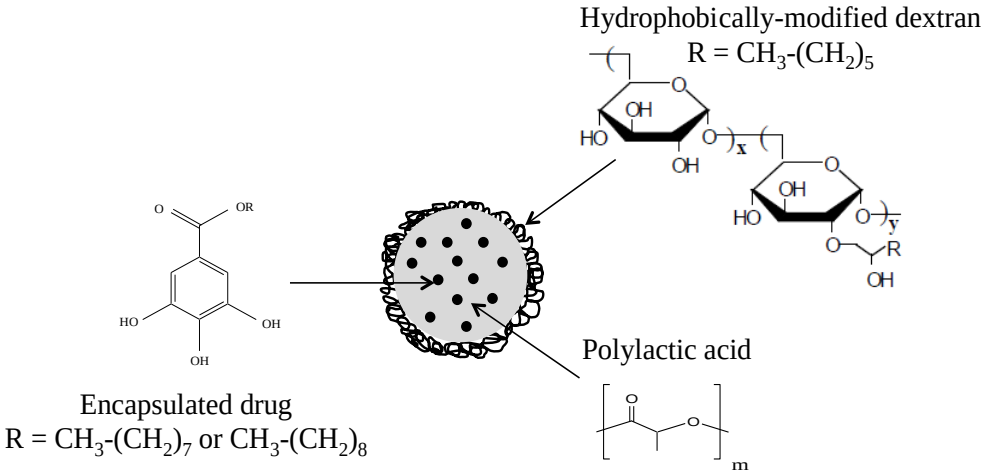

Figure 1b

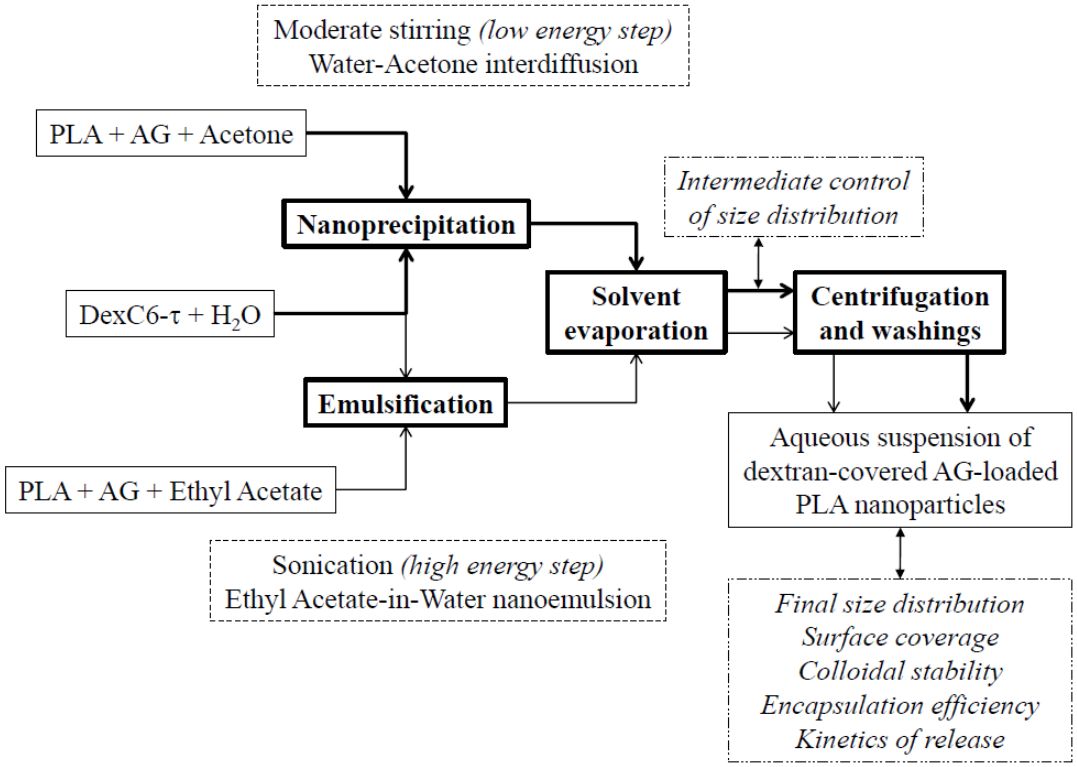

Figure 2

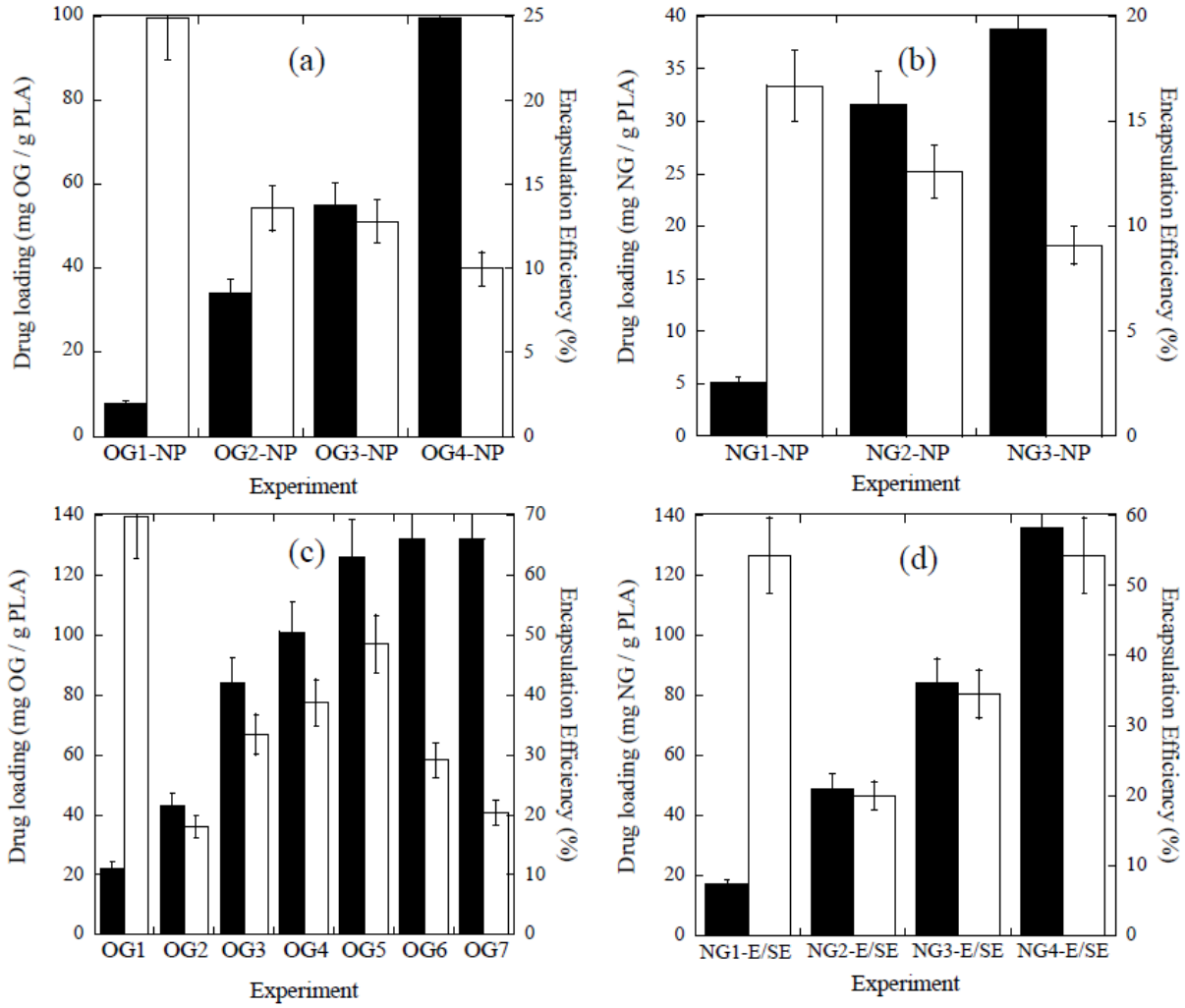

Figure 3a

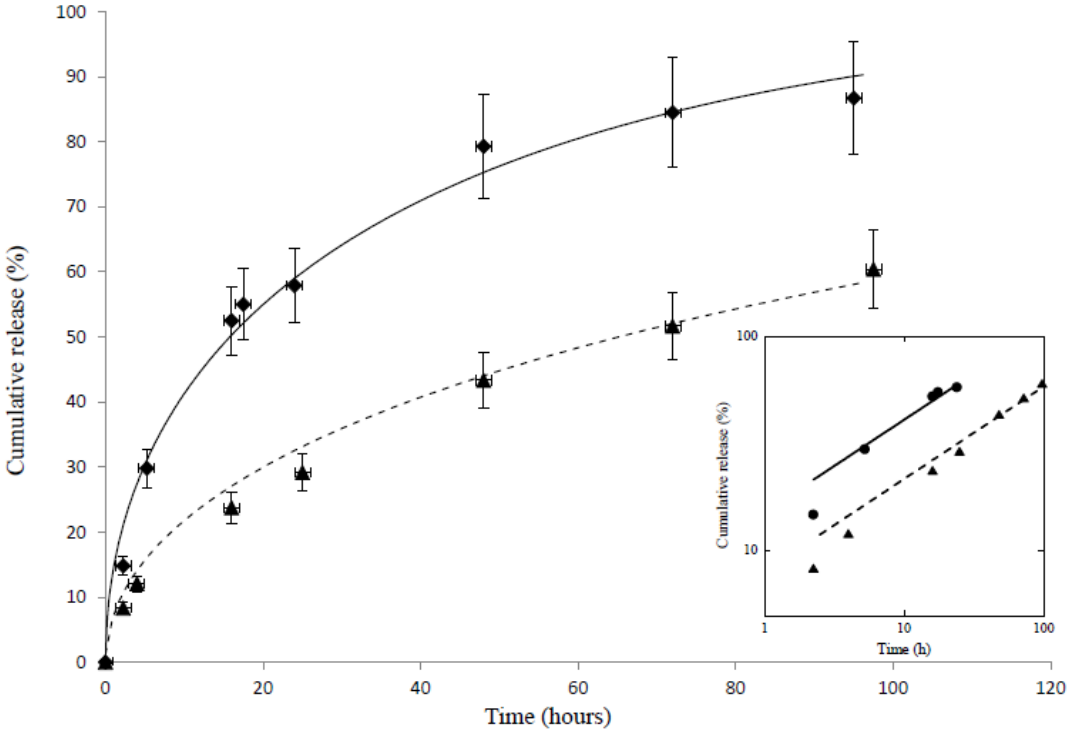

Figure 3b

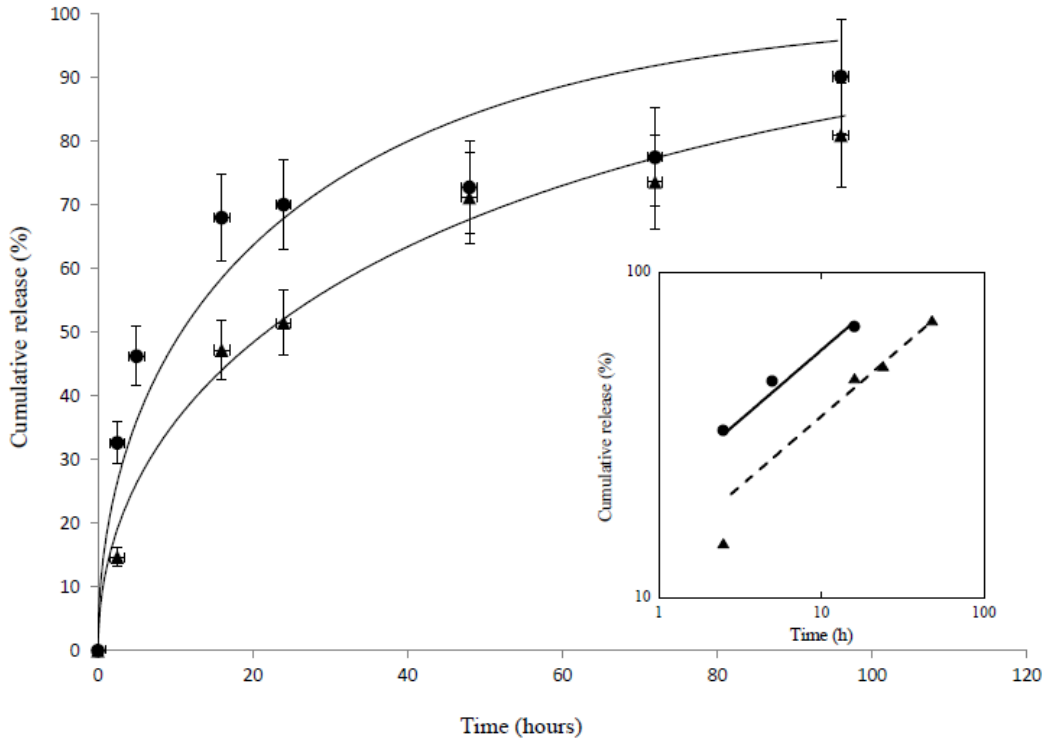

Table 1: Characteristics of nanoparticles prepared by both processes as a function of the substitution ratio (τ) of $DexC_6$-τ dissolved in the initial aqueous phase (10 g/L). All experiments were repeated between 2 and 3 times.

Process[a]	**τ (%)**	**d(0.5)**[b] **(nm)**	**D[3,2]**[b] **(nm)**	**Span**	**Γ**[c]**±0.5 (mg/m²)**	**CCA**[d] **(M)**
NP	14	148	127	1.1	2.3	≤ 1M
	16	143	130	1.0	2.2	≤ 1M
	17	158	139	1.0	2.5	≤ 1M
	21	141	130	0.9	2.8	$\leq 10^{-2}$M
E/SE	16	96	94	0.9	3.4	≤ 1M
	20	93	83	1.1	3.3	≤ 1M
	22	116	112	1800	nd	$\leq 10^{-2}$M

[a] NP: nanoprecipitation (organic phase 5 mL acetone, PLA 10 g/L and aqueous phase 10 mL $DexC_6$-τ 10 g/L). E/SE: emulsion/solvent evaporation (organic phase 2 mL AcOEt, PLA 50 g/L and aqueous phase 10 mL $DexC_6$-τ 10 g/L).

[b] The relative uncertainty on particle diameter was ± 10 %.

[c] Surface coverage of particles by $DexC_6$-τ.

[d] NaCl critical concentration of particle aggregation.

Table 2a: Effect of loaded AG amount in the initial organic phase on the size distribution of AG-loaded PLA nanoparticles obtained by NP, before and after the centrifugation and washing steps. All experiments were repeated between 2 and 3 times.

		Before centrifugation & washings			**After centrifugation & washings**			
Sample	**AG[a] (wt %)**	**d(0.5)[b] (nm)**	**D[3,2][b] (nm)**	**Span**	**d(0.5)[b] (nm)**	**D[3,2][b] (nm)**	**Span**	**Γ[c]±0.5 (mg/m^2)**
OG1-NP	3	140	125	1.1	163	162	0.7	2.2
OG2-NP	20	164	146	1.1	172	178	0.9	nd
OG3-NP	30	134	120	1.1	145	140	1.0	2.0
OG4-NP	50	131	119	1.0	173	170	90.0	2.3
NG1-NP	3	139	125	1.0	160	153	0.7	2.4
NG2-NP	20	124	112	1.1	134	118	1.2	1.9
NG3-NP	30	125	111	1.2	138	119	1.2	1.8

[a] Total PLA and AG amount: 50 mg in 5 mL acetone, aqueous phase 10 mL DexC_6-τ, 10 g/L.

[b] The relative uncertainty on particle diameter was ± 10 %.

[c] Surface coverage of particles by DexC_6-τ.

Table 2b: Effect of loaded AG amount in the initial organic phase and AG + PLA amount on the size distribution of AG-loaded PLA nanoparticles obtained by E/SE, before and after the centrifugation and washing steps. All experiments were repeated between 2 and 3 times.

			Before centrifugation & washings			**After centrifugation & washings**			
Sample	**AG (wt %)**	**AG+PLA (mg)**	**d(0.5)[a] (nm)**	**D[3,2][a] (nm)**	**Span**	**d(0.5)[a] (nm)**	**D[3,2][a] (nm)**	**Span**	**$\Gamma^{d}\pm0.5$ (mg/m^2)**
OG1-E/SE	3	200 [b]	134	116	1.3	146	126	1.2	2.0
OG2-E/SE	20	50 [c]	107	101	1.1	99	91	1.1	2.4
OG3-E/SE	20	100 [b]	91	80	1.1	91	80	1.1	2.6
OG4-E/SE	20	200 [b]	108	96	1.4	113	99	1.2	2.0
OG5-E/SE	20	300 [b]	126	108	1.5	128	114	4.4	3.0
OG6-E/SE	30	100 [b]	96	86	1.2	120	116	158.0	2.5
OG7-E/SE	40	100 [b]	99	90	1.2	121	110	52.0	2.5
NG1-E/SE	3	200 [b]	126	122	0.9	117	109	1.2	2.5
NG2-E/SE	20	50 [c]	102	94	1.2	105	96	1.1	2.0
NG3-E/SE	20	100 [b]	94	86	1.0	113	103	1.8	2.6

NG4-E/SE	20	200 [b]	101	89	1.2	193	196	6.8	4.2
NG5-E/SE	20	300[b]	128	113	1.2	230	264	36.7	4.1

[a] The relative uncertainty on particle diameter was ± 10 %.

[b] In 2 mL EA, aqueous phase 10 mL DexC_6-τ, 10 g/L, saturated with EA.

[c] In 5 mL EA, aqueous phase 10 mL DexC_6-τ, 10 g/L, saturated with EA.

[d] Surface coverage of particles by DexC_6-τ.

Table 2c: Comparison of characteristics of NG-loaded nanoparticles prepared by NP and E/SE process with the same formulation parameters except the nature of the organic solvent. The aqueous phase was 10 mL of 10 g/L DexC_6-18 solution. For NP process the organic phase contained 5 mL acetone + 40 mg PLA + 10 mg NG. For E/SE process, the organic phase contained 6 mL EA + 40 mg PLA + 10 mg NG.

Process	**d(0.5)[a] (nm)**	**D[3,2][a] (nm)**	**Span**	**Γ[b] (mg DexC_6-18 / m^2)**	**Drug loading[c] (mg NG / g PLA)**	**EE[c] (%)**	**CCA[d] (M)**	**Δ_{PZ}[e] (nm)**
NP	159	143	1.0	2.0	32.9	13.2	1	10
E/SE	104	96	1.2	2.5	49.4	19.8	1	10

[a] The relative uncertainty on particle diameter was ± 10 %.

[b] Surface coverage of particles by DexC_6-18. The uncertainty was ± 0.5 mg/m^2.

[c] The relative uncertainty on drug loading and encapsulation efficiency was ± 10 %.

[d] NaCl critical concentration of particle aggregation.

[e] Electrokinetic layer thickness of superficial DexC_6-18 layer (**Equation (3)**). The uncertainty was ± 2 nm.

Table 3: Values of "apparent partition coefficient" for both AGs and both processes (for definition and discussion see text).

AG	Process	
	NP	**E/SE**
OG	43	46
NG	31	69

Table 4a: Diffusion coefficient of AG within nanoparticles prepared by NP or E/SE (See **Table 2a** and **2b** for conditions of preparation).

Sample	**Drug loading[a]** **(mg SA / g PLA)**	***D*** **(10^{-21} m^2/s)**
OG1-NP	10.2	6.5
OG2-NP	28.2	5.2
NG1-NP	5.1	2.1
NG2-NP	32.0	2.0
OG1-E/SE	21.6	1.6
OG2-E/SE	43	1.1
OG4-E/SE	99.0	2.5
NG1- E/SE	16.9	0.1
NG2-E/SE	52.3	0.3

[a] The relative uncertainty on drug loading was ± 10 %.

Table 4b: Reported values of diffusion coefficients of various hydrophobic molecules in PLA nanoparticles.

Process	**Encapsulated molecule**	**Diameter of nanoparticles (nm)**	***D*** **(m^2/s)**	**Reference**
E/SE	Haloperidol	220	$5.1\ 10^{-23}$	[64]
	Lidocaine	205	$7.7\ 10^{-20}$	[28]
	Lidocaine	225	$5.2\ 10^{-20}$	[65]
	4-nitroanisol	511	$4.9\ 10^{-19}$	[66]
NP	Tyrphostin AG-1295	170	$2.0\ 10^{-20}$	[67]